ChemComm

Accepted Manuscript

This article can be cited before page numbers have been issued, to do this please use: X. Ma, Y. Chen, H. Wang, Q. Li, W. Lin and W. Cai, *Chem. Commun.*, 2018, DOI: 10.1039/C7CC08793D.

ROYAL SOCIETY OF CHEMISTRY

rsc.li/chemcomm

View Article Online
DOI: 10.1039/C7CC08793D

Journal Name

COMMUNICATION

Electrocatalytic Oxidation of Ethanol and Ethylene Glycol on Cubic, Octahedral and Rhombic Dodecahedral Palladium Nanocrystals

Received 00th January 20xx,
Accepted 00th January 20xx

DOI: 10.1039/x0xx00000x

www.rsc.org/

Xian-Yin Ma[a,c], Yafeng Chen[b], Han Wang[c], Qiao-Xia Li[a], Wen-Feng Lin[*b], Wen-Bin Cai[*c,a]

Cubic, octahedral and rhombic dodecahedral Pd nanocrystals were synthesized and examined as nanocatalysts for electro-oxidation of ethanol and ethylene glycol. Combined electrochemical measurements and density functional theory calculations reveal that nanofacet-dependent affinity and reactivity of OH_{ads} and CO_{ads} are closely linked to the C2 alcohol oxidation activities, with the highest reactivity found on the Pd nanocubes bounded by {100} facets.

Ethanol and ethylene glycol based direct alcohol fuel cells are particularly attractive for portable power applications, owing to their theoretically high energy densities, low toxicity and facile generation of the fuels from biomass.[1, 2] Alternatively, alcohol electro-reforming is an energy-efficient, low cost and environmentally friendly technology to produce clean hydrogen at the cathode and valuable chemicals from biomass-derived alcohol oxidation at the anode, in a simple electrolysis cell at low temperature and atmospheric pressure.[3] For both of the fuel cell and hydrogen technologies, the efficient oxidation of the C2 alcohol by means of electrocatalysis is essential, and the efficiency is largely determined by the catalysts employed.

Due to the rarity and high cost of Pt, Pd-based catalysts have been investigated as alternative promising catalytic materials for C2 alcohol oxidation in alkaline media given that they compete with traditional Pt-based ones in term of electrocatalytic activities at high pH.[4-7] Although significant technical progress has been achieved on anion exchange membranes for the direct alkaline alcohol fuel cells and the alcohol reforming electrolytic cells, oxidation of C2 alcohols on Pd surfaces has received far less attention than that on Pt surfaces,[8, 9] hindering the development of more efficient Pd-based catalysts.

Facet control is one of the effective tactics to attain surface structure manipulation that may lead to the design of high performance catalysts.[10-12] Studies on Pd bulk single crystals have shown that the crystallographic orientations can have significant impacts on the electrocatalysis of formic acid oxidation and oxygen reduction.[13-15] The three basal planes (111), (100) and (110), are of fundamental interest since they may be combined to constitute structurally higher index planes of single crystals.[16] It has been reported that the formic acid oxidation activity on Pd single crystals increases in the order of Pd(111) < Pd(110) < Pd(100) in sulfuric acid solution,[13] while the oxygen reduction activity follows the order of Pd(110) < Pd(111) < Pd(100) in perchloric acid solution.[14]

From the practical viewpoint, Pd nanocrystals are much more preferred to be employed as the catalysts compared to Pd bulk crystals.[17] The preferential nanofacets could be created by tailoring the shapes of nanocrystals, e.g., Pd cubes, octahedrons (Octs) and rhombic dodecahedrons (RDs) are enclosed predominantly by {100}, {111} and {110} nanofacets, respectively.[16] Clearly, a systematic investigation into the electrocatalytic activities of these model Pd nanocatalysts for ethanol and ethylene glycol oxidation in alkaline media is highly demanded and timely for the development of direct alcohol alkaline fuel cells and electro-reforming cells.

Pd cubes, RDs and Octs nanocrystals were obtained via wet chemistry one-pot synthesis[18,19] and then casted on a glassy

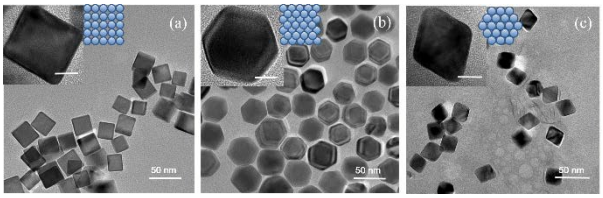

Figure 1. Transmission electron microscopic (TEM) images of Pd cubes (a), RDs (b) and Octs (c). The inserts are the zoomed-in images for single particles at the scale bar of 10 nm, and the corresponding schematic surface atomic arrangements.

[a] Shanghai Key Laboratory of Materials Protection and Advanced Materials in Electric Power, College of Environmental and Chemical Engineering, Shanghai University of Electric Power, Shanghai 200090, China.
[b] Department of Chemical Engineering, Loughborough University, Loughborough, Leicestershire, LE11 3TU, U.K. Email: w.lin@lboro.ac.uk
[c] Shanghai Key Laboratory of Molecular Catalysis and Innovative Materials, Collaborative Innovation Center of Chemistry for Energy Materials, Department of Chemistry, Fudan University, Shanghai 200433, China.
Electronic Supplementary Information (ESI) available. See DOI: 10.1039/c000000x/

carbon electrode for the electrocatalytic evaluation (see ESI† for details).

The transmission electron microscopic (TEM) images of the as-synthesized Pd cubes (a), RDs (b) and Octs (c) with well-defined shape and a high yield/selectivity (> 90%) are shown in Figure 1 and Figure S1. The mean sizes in the edge-length lie around 25.3±2.1, 23.6±2.7 and 21.5±1.9 nm for Pd cubes, RDs and Octs, respectively. More details of nanofacet characterization and the XRD data are shown in Figures S2 and S3, which all support the identified surface structures. As demonstrated in the previous report,[20] Pd nanocrystals of these similar sizes should not have a significant size effect on their specific activities, however the electrochemical properties of Pd nanocrystals are highly dependent on their surface cleanness, and the removal of residual surfactants on the nanocrystals after the wet chemistry synthesis is thus essential for a reliable comparison. Based on our previous reports,[6,19] the removal of CTAB/CTAC residues on Pd nanocrystals supported on glassy carbon electrode was enabled by effectively utilizing the CO-adsorption displacement tactics in a CO-bubbled 0.5 M H_2SO_4 solution at 0.35 V vs RHE for 900 s followed by subsequent anodic CO_{ads} stripping. Figure S4 shows the cleaning treatment effect, which confirms the clean surface was obtained.

Figures 2a and 2b show the cyclic voltammograms (CVs) recorded for surface cleaned Pd nanocrystals in 0.5 M H_2SO_4 and 1.0 M NaOH electrolytes, respectively. In acidic media, the formation/reduction of surface PdO and hydrogen/bisulfate adsorption/desorption current peaks on differently faceted Pd nanocrytals were observed over distinct potential regions, similar to the voltammetric features for the corresponding Pd bulk single crystal electrodes.[21]

Shape-dependent unique voltammetric features for the formation/reduction of PdO and hydrogen adsorption /desorption processes were also observed in alkaline media

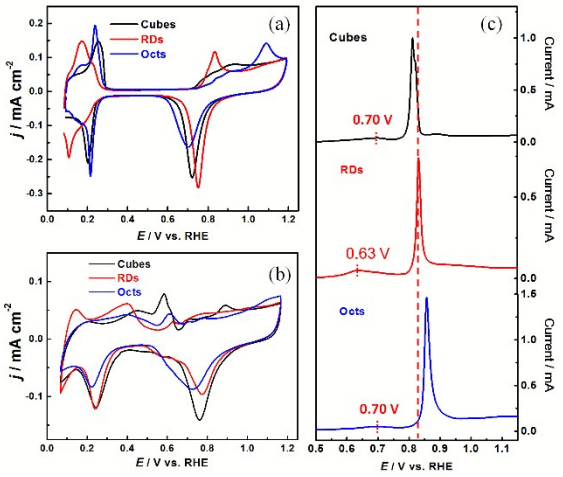

Figure 2. Cyclic voltammograms (CVs) of Pd nanocrystals recorded in 0.5 M H_2SO_4 (a) and 1.0 M NaOH (b) electrolytes, respectively. The CO stripping curves obtained from the three types of Pd nanocrystals in 1.0 M NaOH are also shown here (c). Scan rate: 50 mV s^{-1}. The current densities in (a) and (b) are shown by normalizing the measured currents to the electroactive areas of designated Pd nanocrystals (see text, *vide infra*).

over the high and low potential regions,[22] respectively, see Figure 2b. It has been well documented that OH ions are chemisorbed over a broad potential region before and during the initial stage of the surface oxide layer formation. [22, 23] At potentials below ca. 0.70 V, the redox current peaks appearing in the voltammograms are related to the hydrogen desorption/adsorption and OH adsorption /desorption processes.[9, 24] To get an insight into the OH formation potentials on the different Pd facets, we performed DFT calculations (see ESI† for details of DFT computational method) and the main results are presented in Figure 3, with the supporting adsorption energy data given in the Table S1.

From the DFT simulation on a simplified surface model as explained in the ESI, the onset potential of OH formation on the three basal Pd planes of (111), (100) and (110) are 0.31 V, 0.07 V and -0.13 V, respectively, indicating that the OH adsorption reaction process on Pd(110) surface was firstly initiated for its lowest onset potential, although the calculated values are obviously lower than the experimental ones due to the simplified model. It has been well documented that the adsorption of hydroxyl species was most favoured on Pt(110) followed by Pt(100) and Pt(111).[9] Meanwhile, an indirect experimental evidence comes from the report that O species adsorbed at lowest temperature on Pd(110) followed by Pd(100) and Pd(111) at the solid-gas interface, as detected by XPS.[25] Along this line, the broad peak located at ca. 0.40 V for Pd RDs may be attributed to desorption of hydrogen and adsorption of OH^- to form OH_{ads} on {110} nanofacets. The peaks located at ca. 0.585 and 0.615 V, which are too high for the potential of hydrogen desorption, may be assigned to the chemisorption of OH^- on {100} nanofacets of Pd cubes and {111} nanofacets of Pd Octs, respectively.[15, 26] Since OH_{ads} is the essential reactant pair involved in oxidizing the carbonaceous intermediate species including $CH_3C^*=O$, CO and CH_x during EOR,[23, 27] and $HO\text{-}CH_2C^*=O$, CO and CH_xO during EGOR,[6] the Pd

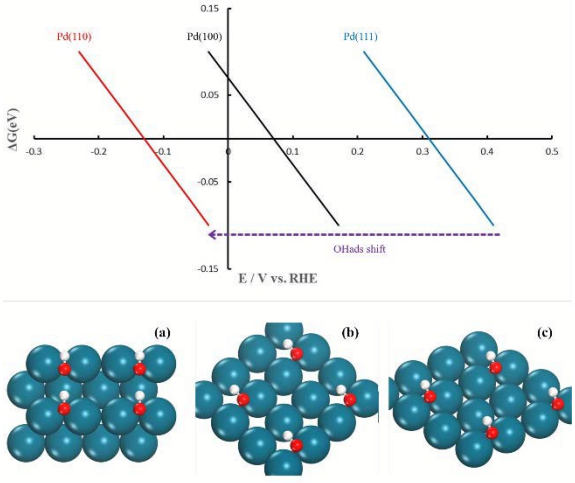

Figure 3. Calculated phase diagram of OH adsorption on Pd(110), Pd(100) and Pd(111) facets. The optimized configurations of OH_{ads} on the bridge sites of the three surfaces are shown in (a) OH_{ads}/Pd(110), (b) OH_{ads}/Pd(100) and (c) OH_{ads}/Pd(100), where red is the O, white is H and blue is Pd atoms.

surface with a relatively facile OH_{ads} formation at a lower potential in general favours CO oxidation, EOR and EGOR. It is worth noting that, OH_{ads} forms with its coverage increasing over a rather wide potential window,[23] its formation is essential but not sufficient for initializing the above oxidation processes. The surface reactivity is also dependent on the activation of C2 reactants and carbonaceous intermediates on different Pd nanofacets.[28] Therefore, the resulting electrocatalytic activity of Pd nanocrystals may vary to some extent case by case for different oxidation reactions.

CO adsorbate (CO_{ads}) is an intermediate species formed from the C-C bond breaking during EOR and EGOR,[6, 27, 29] playing a dual role: one is the reactive species to be further converted to CO_2 via $CO_{ads} + OH_{ads} => CO_2 + H^+ + e^-$ (further to carbonate in a high pH alkaline solution), and the other is the poisonous species to block surface active sites for other parallel reactions.[27,30] For the pre-dosed CO_{ads} monolayer on Pd nanocrystals, the anodic oxidation stripping voltammograms in N_2-deaerated 1.0 M NaOH solution (Figure 2c) revealed that the CO_{ads} oxidation on Pd nanocrystals occurs in two distinct potential regions, as demonstrated by the oxidation pre-peak and the main oxidation peak. The pre-peak may arise from the reaction of weakly adsorbed CO (for example, part of linear adsorbed CO, or CO_L) with OH_{ads} formed at lower potentials. In fact, CO adsorption on Pd surfaces may take linear (CO_L), bridge (CO_B) and hollow (CO_H) sites, with increasing CO adsorption strength. The preference of which depends greatly on Pd crystalline orientation. An IR spectroscopy study[31] suggests that despite the highest CO_B band observed on Pd(100), (111) and (110), relatively higher portion of CO_L is present on Pd(110), CO_B on Pd(100), and CO_H on Pd(111), respectively. Therefore, the main oxidation current peak could be attributed to the reaction of the majority of CO_{ads} with sufficiently high coverage and active OH_{ads} on Pd surfaces.[32-34]

The CO oxidation pre-peak appears at *ca*. 0.63, 0.70 and 0.70 V for Pd RDs, cubes and Octs, respectively, being consistent with the adsorption strengths of OH_{ads} and CO_{ads} on the three basal planes. Nevertheless, the main oxidation peak on Pd cubes materializes at 0.810 V, was earlier than that on both Pd RDs (0.832 V) and Pd Octs (0.857 V). The slightly delayed oxidation of the majority of CO_{ads} on Pd RDs may be caused by the reduced mobility of CO_{ads}, as well as that of OH_{ads}, on the stepped {110} surface, as compared to that on flat {111} and {100}.[30]

On the other hand, the total charge associated with CO_{ads} stripping may be used to evaluate the exposed electroactive surface areas, that is, 1.08, 2.13 and 0.96 cm^2 for Pd cubes, Octs and RDs, casted on glassy carbon electrode, respectively. Therefore, for a reasonable comparison, all the electro-chemical current densities presented in this work except those in Figure 2c were respectively normalized to the electroactive areas of the designated Pd nanocrystals to represent their inherent specific activities.

As compared to the CO_{ads} oxidation, the EOR on Pd electrodes in alkaline media is more complicated, proceeding through the so-called C1 and C2 pathways,[27, 29] in which the minor C1 pathway involves the C-C bond breaking to form CO_{ads} and CH_x surface species at lower potentials, followed by their further oxidation to CO_2 (CO_3^{2-}) at higher potentials. The majority of CO_{ads} species would not start to be further oxidized until the potential is raised higher than *ca*. 0.77 V, as can be seen from Figure 2c. Meanwhile, the predominant C2 pathway may proceed via $CH_3C^*=O + OH_{ads} + OH^- => CH_3COO^- + H_2O$ to form acetate,[27] the acetate may adsorb at the surface to become additional poisoning species at a sufficiently higher potential.[9]

Figure 4(a) shows CVs for Pd nanocrystals in 1 M NaOH + 1 M ethanol solution, in which Pd cubes exhibit the highest peak current density, followed by Pd Octs and Pd RDs. The highest oxidation peak current density on Pd cubes seems consistent with both the lowest barrier for dehydrogenation of ethanol on Pd(100) indicated by the DFT calculation[35], and the favourable subsequent oxidation of the majority of $CH_3C^*=O$ and CO_{ads} intermediates on Pd cubes, inferred from the previous mechanism study[4,27] and the above CO stripping measurement. In terms of nanofacet dependence, the oxidation onset potential and peak potential for EOR are the lowest on Pd RDs, as compared to those on Pd cubes and Pd Octs, due to the lowest potential for OH^- chemisorption on {110} nanofacets. Further chrono-amperometric measurement in the same electrolyte indicated the highest EOR oxidation current density maintained on Pd cubes after anodic polarization at 0.67 V for 3600 s. In fact, 41%, 18% and 13% of the initial current densities were sustained on Pd cubes, RDs and Octs, respectively (see Figure 4b). The most durable EOR activity on Pd cubes at 0.67 V, as demonstrated in Figure 4b, may arise from the least accumulation of both CO_{ads} and adsorbed acetate species. Otherwise, increasing CO_{ads} and acetate coverage may block surface active sites during EOR, resulting in the quicker decay of current densities.

EGOR on Pd electrode in alkaline media seems even more complicated than that for EOR, with the main products being glycolate and glyoxal in the C2 pathway and the minor product being CO_2 or its derivatives in the C1 pathway besides the surface intermediates $HO\text{-}CH_2C^*=O$, CO_{ads} and CH_xO_{ads}.[6]

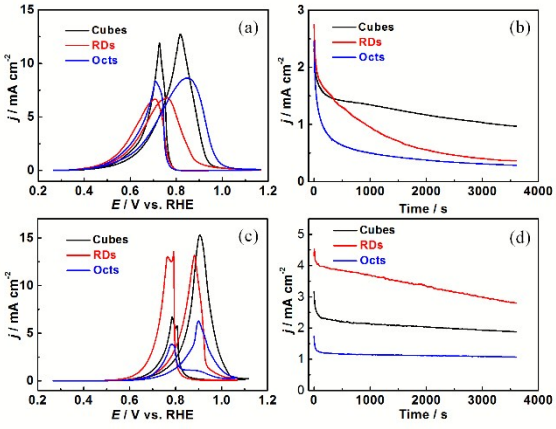

Figure 4. Cyclic voltammograms (CVs) (a) and chronoamperometric curves at 0.67 V (b) recorded for Pd nanocrystals in 1.0 M NaOH + 1.0 M ethanol; CVs (c) and chronoamperometric curves at 0.82 V (d) recorded for Pd nanocrystals in 1.0 M NaOH + 1.0 M ethylene glycol. Scan rate for all the CVs: 50 mVs^{-1}. The current densities are shown by normalizing the measured currents to the electroactive areas of designated Pd nanocrystals.

In analogy to the role of $CH_3C^*=O$ in EOR at Pd,[27] our previous spectroelectrochemical study indicates that $HO\text{-}CH_2C^*=O$ acts as the pivotal intermediate for the C2 and C1 pathways in EGOR on Pd in alkaline media.[6] Figure 4c shows the corresponding CVs for Pd nanocrystals in 1 M NaOH + 1 M ethylene glycol solution. The oxidation peak current densities followed the order of Pd cubes > RDs > Octs, with the onset oxidation potentials shifting positively by nearly 0.20 V, compared to the counterparts in the case of EOR. This potential shift could be attributed to higher CO_{ads} coverages resulting from enhanced C-C bond cleavage of ethylene glycol versus that of ethanol on Pd surfaces.[36] In analogy to the explanations for EOR, the lowest onset potential and peak potential for EGOR on Pd(110) may be attributable to the lowest potential for OH_{ads} formation, whilst the highest oxidation peak current on Pd cubes may arise from both the most favoured dehydrogenation of ethylene glycol and the facile subsequent oxidation of the majority of $HO\text{-}CH_2C^*=O$ and CO_{ads} intermediates on {100} nanofacets. After anodic polarization at 0.82 V for 3600s (Figure 4d), the current densities of EGOR on Pd cubes, RDs and Octs remained 64%, 64%, 61% of their initial values, respectively. The relatively higher durability seen in Figure 4d than that in Figure 4b is likely due to the fact that CO_{ads} oxidative removal at 0.82 V was more facile than that at 0.67 V due to weaker CO_{ads} bonding to the surface at the higher potential.[33] In addition, a closer look at Figure 4d reveals that the oxidation current decayed at a larger slope for EGOR on Pd RDs than on Pd cubes after 100 s, despite a higher current due to the lowest onset potential on Pd RDs as seen in Figure 4c. This observation suggests that Pd cubes are more suitable for longer operation in EGOR (see ESI for the discussion on this).

In conclusion, both ethanol oxidation reaction (EOR) and ethylene glycol oxidation reaction (EGOR) on nano-sized Pd cubes, octahedrons (Octs) and rhombic dodecahedrons (RDs) in alkaline media have been demonstrated to be nanofacet sensitive. The electrocatalytic activities in terms of oxidation peak current densities follow the sequence of cubes > Octs > RDs for EOR and that of cubes > RDs > Octs for EGOR. The nanofacet dependent affinity and reactivity of OH_{ads} and CO_{ads} significantly affect the EOR and EGOR on differently shaped Pd nanocrystals. The highest electrocatalytic activities of EOR and EGOR on Pd cubes may be ascribed to the most favoured dehydrogenation and subsequent oxidation of majority of (hydroxyl)acetyl and CO_{ads} intermediates on {100} nanofacets, whilst the lowest onset and peak potentials of EOR and EGOR on Pd RDs were attributed to the formation of OH_{ads} at the lowest potential on Pd{110} nanofacets. The current finding suggests clearly that Pd nanocubes are the choice of catalysts for direct C2 alcohol alkaline fuel cells as well as C2 alcohol electro-reforming cells for hydrogen production.

This work is supported by the NSFC (No. 21473039 and 21733004), the 973 Program of MOST (No. 2015CB932303) and the UK EPSRC (EP/I013229/1).

Conflicts of interest

There are no conflicts to declare.

Notes and references

View Article Online
DOI: 10.1039/C7CC08793D

1 C. Bianchini and P. K. Shen, *Chem Rev*, 2009, **109**, 4183-4206.
2 H. Yue, Y. Zhao, X. Ma and J. Gong, *Chem Soc Rev*, 2012, **41**, 4218-4244.
3 Y. X. Chen, A. Lavacchi, H. A. Miller, M. Bevilacqua, J. Filippi, M. Innocenti, A. Marchionni, W. Oberhauser, L. Wang and F. Vizza, *Nat Commun*, 2014, **5,** 4036-4042.
4 Y. Wang, S. Z. Zou and W. B. Cai, *Catalysts*, 2015, **5**, 1507-1534.
5 L. L. Zhang, Q. W. Chang, H. M. Chen and M. H. Shao, *Nano Energy*, 2016, **29**, 198-219.
6 H. Wang, B. Jiang, T. T. Zhao, K. Jiang, Y. Y. Yang, J. W. Zhang, Z. X. Xie and W. B. Cai, *ACS Catal*, 2017, **7**, 2033-2041.
7 W. J. Huang, X. Y. Ma, H. Wang, R. F. Feng, J. G. Zhou, P. N. Duchesne, P. Zhang, F. J. Chen, N. Han, F. P. Zhao, J. H. Zhou, W. B. Cai and Y. G. Li, *Adv Mater*, 2017, **29**. 1703057.
8 C. Buso-Rogero, S. Brimaud, J. Solla-Gullon, F. J. Vidal-Iglesias, E. Herrero, R. J. Behm and J. M. Feliu, *J Electroanal Chem*, 2016, **763**, 116-124.
9 C. Buso-Rogero, E. Herrero and J. M. Feliu, *ChemPhysChem*, 2014, **15**, 2019-2028.
10 N. Tian, Z. Y. Zhou, N. F. Yu, L. Y. Wang and S. G. Sun, *J Am Chem Soc*, 2010, **132**, 7580-7581.
11 J. W. Zhang, L. Zhang, S. F. Xie, Q. Kuang, X. G. Han, Z. X. Xie and L. S. Zheng, *Chem-Eur J*, 2011, **17**, 9915-9919.
12 T. T. Zhao, H. Wang, X. Han, K. Jiang, H. X. Lin, Z. X. Xie and W. B. Cai, *J Mater Chem A*, 2016, **4**, 15845-15850.
13 M. Baldauf and D. M. Kolb, *J Phys Chem*, 1996, **100**, 11375-11381.
14 S. Kondo, M. Nakamura, N. Maki and N. Hoshi, *J Phys Chem C*, 2009, **113**, 12625-12628.
15 M. H. Shao, J. Odell, M. Humbert, T. Y. Yu and Y. N. Xia, *J Phys Chem C*, 2013, **117**, 4172-4180.
16 N. Tian, Z. Y. Zhou and S. G. Sun, *J Phys Chem C*, 2008, **112**, 19801-19817.
17 Y. C. Yan, J. S. S. Du, K. D. Gilroy, D. R. Yang, Y. N. Xia and H. Zhang, *Adv Mater*, 2017, **29**.
18 W. X. Niu, L. Zhang and G. B. Xu, ACS Nano, 2010, 4, 1987-1996.
19 H. X. Zhang, H. Wang, Y. S. Re and W. B. Cai, *Chem Commun*, 2012, **48**, 8362-8364.
20 M. S. Jin, H. Zhang, Z. X. Xie and Y. N. Xia, *Energ Environ Sci*, 2012, **5**, 6352-6357.
21 M. Hara, U. Linke and T. Wandlowski, *Electrochim Acta*, 2007, **52**, 5733-5748.
22 N. Hoshi, M. Nakamura, N. Maki, S. Yamaguchi and A. Kitajima, *J Electroanal Chem*, 2008, **624**, 134-138.
23 Z. X. Liang, T. S. Zhao, J. B. Xu and L. D. Zhu, *Electrochim Acta*, 2009, **54**, 2203-2208.
24 Y. Katayama, T. Okanishi, H. Muroyama, T. Matsui and K. Eguchi, *ACS Catal*, 2016, **6**, 2026-2034.
25 H. Kondoh, R. Toyoshima, Y. Monya, M. Yoshida, K. Mase, K. Amemiya and B. S. Mun, *Catal Today*, 2016, **260**, 14-20.
26 J. S. Ye, S. Y. Hsu and C. L. Lee, *Electrochim Acta*, 2016, **211**, 1024-1032.
27 Y. Y. Yang, J. Ren, Q. X. Li, Z. Y. Zhou, S. G. Sun and W. B. Cai, *ACS Catal*, 2014, **4**, 798-803.
28 R. Cortese, R. Schimmenti, F. Ferrante, A. Prestianni, D. Decarolis and D. Duca, *J Phys Chem C*, 2017, **121**, 13606-13616.
29 E. A. Monyoncho, S. N. Steinmann, C. Michel, E. A. Baranova, T. K. Woo and P. Sautet, *ACS Catal*, 2016, **6**, 4894-4906.
30 F. Maillard, E. R. Savinova and U. Stimming, *J Electroanal Chem*, 2007, **599**, 221-232.
31 N. Hoshi, O. Koga, Y. Hori and T. Ogawa, *J Electroanal Chem*, 2006, **587**, 79-85.
32 T. Sheng, W. F. Lin, C. Hardacre and P. Hu, *J Phys Chem C*, 2014, **118**, 5762-5772.
33 B. Y. Liu, J. M. Jin, C. Hardacre, P. Hu and W. F. Lin, *J Electroanal Chem*, 2013, **688**, 216-223.
34 J. M. Jin, T. Sheng, X. Lin, R. Kavanagh, P. Hamer, P. J. Hu, C. Hardacre, A. Martinez-Bonastre, J. Sharman, D. Thompsett and W. F. Lin, *Phys Chem Chem Phys*, 2014, **16**, 9432-9440.
35 E. D. Wang, J. B. Xu and T. S. Zhao, *J Phys Chem C*, 2010, **114**, 10489-10497.
36 J. L. Lin, J. Ren, N. Tian, Z. Y. Zhou and S. G. Sun, *J Electroanal Chem*, 2013, **688**, 165-171.

View Article Online
DOI: 10.1039/C7CC08793D

Graphical abstract

Ethanol and ethylene glycol electrocatalytic oxidation on Pd cubic, octahedral and rhombic dodecahedral nanocrystals in alkaline media was systematically investigated.